16.5

Numerical Simulation of Tornadogenesis in a Supercell Storm

Ken-ichi Shimose and Tetsuya Kawano

Department of Earth and Planetary Sciences, Kyushu University, Fukuoka, Japan

1. Introduction

Supercells are highly productive of severe weather, and often spawn tornadoes. However, Burgess (1997) reported that only 20% of supercells are associated with tornadoes. Wakimoto et al. (1998) pointed out that a preexisting boundary played an important role in the tornadogenesis of the Garden City storm during VORTEX (Verification of the Origins of Rotation in Tornadoes Experiment) 95. Using a numerical model with idealized conditions, Atkins et al. (1999) confirmed the importance of preexisting boundary for tornadogenesis associated with supercells. However, numerical simulations with idealized conditions present limitations in discussing the process of tornadogenesis. Therefore, we simulate tornadoes associated with a supercell using a super-high resolution numerical model with realistic conditions and investigate tornadogenesis associated with the supercell.

In the present study, we describe results of a numerical simulation of two tornadoes and strong winds associated with a supercell storm which occurred in Saga Prefecture, Japan on 27 June 2004.

2. 27 June 2004 case overview

A supercell on 27 June 2004 generated two tornadoes and strong winds between Saga City and Tosu City. The first tornado, estimated F2 (50 $\sim$ 69 m s^{-1}) in the Fujita scale, occurred in Saga City between 0717 and 0724 JST (Japan Standard Time = UTC + 9 hours). The length of the damage path was about 8 km and its average width was about 200 m. The second tornado, estimated F1 (33 $\sim$ 49 m s^{-1}), was spawned in Tosu City around 0750 JST. The length of the damage path was about 1 km and its average width was about 40 m. In addition, the slight damage occurred due to strong winds between two tornadoes.

Figure 1 shows radar echo in the tornadic phase of the storm. The echo region existed along a quasi-stationary front (Baiu front) which extended from China to the east sea of Japan. The storm of interest in this study began to develop between 0530 and 0600 JST 27 June within the frontal zone east of Goto Islands and propagated east-northeastward. Between 0600 and 0620 JST the storm passed over Sasebo City and caused heavy rainfall (34 mm per 20-min). In the next hour, the storm evolved into a bow-echo and reached Saga City at 0720 JST. Around this time, the storm generated the first tornado at the southwestern edge of the bow-echo. Although the storm declined after the first tornado, it subsequently reintensified and generated the second tornado at 0750 JST in Tosu City. As the first tornado, the second tornado was spawned at the southwestern edge of the storm. After the second tornadogenesis, the storm continued a slight development until 0900 JST and it decayed and disappeared by 1000 JST. The storm moved east-northeastward at a speed of about 13 m s^{-1} throughout its lifetime.

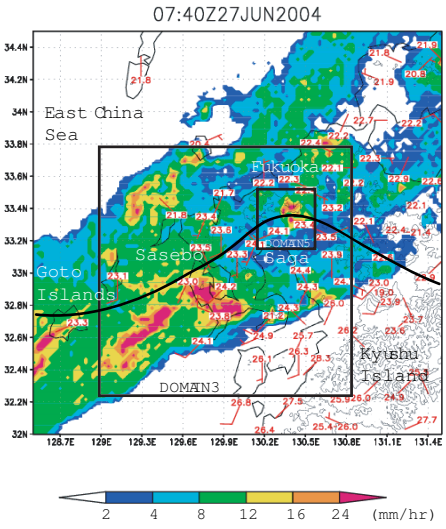

Figure 1: Radar echo at 0740 JST. The horizontal wind (barb) and temperature at the surface are superposed. Baiu front is indicated by bold curve. DOMAIN 3 and 5 are marked by bold lines.

3. Model description and configuration

The 5th generation of the Pennsylvania State University-National Center for Atmospheric Research Mesoscale Model (MM5) version 3.6, three-dimensional, compressible, nonhydrostatic model was used for the simulation. The explicit grid-scale microphysics followed the Goddard microphysics parameterization (Tao et al. 1993). This predicts fields of cloud water, rain water, snow, ice and graupel explicitly with microphysical processes. No cumulus parameterization was used in the simulation. The MRF PBL (Hong and Pan 1996) was employed for the planetary boundary layer. The model initial conditions and time-dependent lateral boundary conditions were derived from the objective analysis data, Meso-ANALysis (MANAL) produced by the Japan Meteorological Agency (JMA). These datasets assimilate the JMA spectral model analysis into the observational data. The resolution of these datasets is 10 km for the horizontal grid spacing and 19 levels in vertical. In the simulation presented here, five domains were required to capture the full range of scales (Table 1, Fig. 1). For all domains, there are 39 full sigma levels from the surface to 100 hPa.

The simulation was started at 2100 JST 26 June 2004 and finished at 1500 JST 27 June. DOMAIN 2 began at 0400 JST and ended at 1000 JST. DOMAIN 3-4 started at 0500 JST and ended at 0830 JST. DOMAIN 2-4 were added in order to capture the storm scale fields. DOMAIN 5 was added from 0710 to 0810 JST to capture the tornado scale fields. For DOMAIN 5, a history file is saved every minute in order to facilitate accurate trajectory calculations and other analysis.

Table 1: Summary of the grid configuration used in the simulation.

	Grid points	Grid spacing
DOMAIN 1	202×202	3.0 km
DOMAIN 2	202×202	1.0 km
DOMAIN 3	202×202	0.9 km
DOMAIN 4	301×301	0.3 km
DOMAIN 5	502×502	0.1 km
Vertical grid	38 levels,	stretching grid

4. Simulated storm overview

The simulated storm undergoes the complex evolution. The evolution of the simulated storm at mid-levels is presented in Figs. 2 and 3. At 0500 JST, the first convective cell (hereafter denoted as C1) is initiated at the kink of the convergence zone associated with the Baiu front. C1 moves east-northeastward and passes over Sasebo City between 0530 and 0550 JST. Although the simulated storm reaches Sasebo City about 30 minutes earlier than the observed storm, the simulated storm path is similar to that of the observed storm. The magnitude of the mid-level vertical vorticity exceeds 0.01 s^{-1} which value is the threshold of the mesocyclone of the supercell (Doswell and Burgess 1993). C1 exhibits the S-shaped structure, which is a characteristic of HP supercell (Moller et al. 1994). C1 maintains its strength in a quasi-steady fashion for the next 30-min, and subsequently decays.

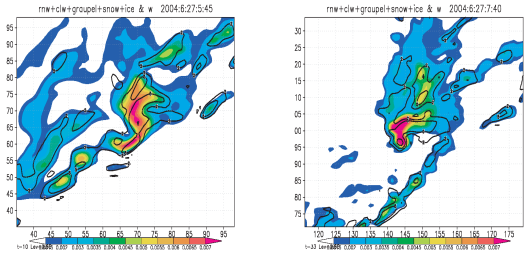

(a) 0545 JST (b) 0740 JST

Figure 2: Horizontal cross sections of the condensate and vertical velocity fields at z = 3 km from DOMAIN 3. The condensate field is indicated by shaded area and the vertical velocity field is indicated by contour. A 65 km × 65 km portion of the full domain is shown, this window moves with the storm.

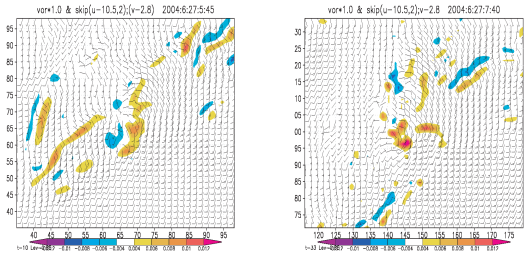

(a) 0545 JST (b) 0740 JST

Figure 3: Same as in Fig. 2 except for the vertical vorticity (shaded) and the storm-relative wind (barbs) fields.

At 0535 JST, the second convective cell (hereafter C2) is initiated on the shear line southwest of the developing C1. C2 approaches C1 with developing. However, C2 does not exhibit the HP supercell-like structure as C1. After 0635 JST, C2 starts decaying and updrafts of C1 and C2 are weaken temporarily. By 0725 JST, C1 and C2 reach Saga City, and the precipitation and updraft cores of C1 and C2 merge into a large single cell. At 0740 JST, the merged cell exhibits a hook-shaped structure. After the merger, the circulation of the merged cell intensifies and then sustains its intensity for about 1.5-hr.

5. Structure and evolution of simulated tornadoes

In this section, we describe the structure and evolution of simulated tornadoes using the data of DOMAIN 5 which horizontal resolution is 100 m. Several strong vortices are simulated, and three of them develop into the strength of F1 tornado (horizontal wind near the surface exceeds 32 m s^{-1}). We mainly focus on the most developed tornado vortex.

Figure 4 presents the condensate and horizontal wind fields near the surface at 0745 JST when the low-level vorticity reach 0.58 s^{-1} which is the maximum value in this simulation. At the same time, the horizontal wind speed exceeds 37 m s^{-1}. This significant developed vertical vortex advects the condensate cyclonically from the main precipitating area extended northwest of the vortex. This feature corresponds to the previous observations of tornadoes (e.g. Dowell and Bluestein 2002a,b; Alexander and Wurman 2004).

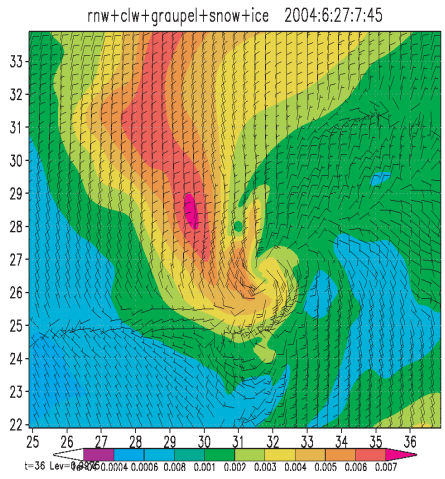

Figure 4: Condensate and horizontal wind fields near the surface at 0745 JST from the DOMAIN 5. The condensate field is indicated by shaded area and horizontal winds are indicated by barbs. A 12 km × 12 km portion of the full domain is shown.

Figures 5 and 6 show evolutions of the vertical velocity field at z = 1 km and the vertical vorticity field near the surface, respectively. At 0743 JST, three regions marked by V0, V1 and V2, exhibiting strong positive vorticity near the surface, are arranged at regular intervals. These vortices are embedded within a vortex sheet accompanied by the convergence zone. This vortex sheet fluctuates and vortices are intensified on crests of the fluctuation. A strong Low-level Updraft (hereafter LU, marked in Fig. 6) is located above V1, and then a strong Mid-level Updraft (hereafter MU, marked in Fig. 6) associated with the mid-level mesocyclone starts to link to LU. At 0745 JST, when MU just links to LU, V1 intensifies into the strongest vortex and exhibits a occluding structure. At 0747 JST, the occluded V1 is cut off from the gust front and decreases the magnitude of vorticity. Characteristics of the evolution of the low-level vortices are summarized as follows; when MU is colocated with LU, updrafts are intensified, subsequently the low-level vorticity is also intensified. This feature suggests that the coupling of the low-level vortex and mid-level mesocyclone is important for the development of the low-level vortex.

We investigate the fluctuation of the vortex sheet shown in a black frame of Fig. 5a. The sheet-width is about 0.3 km, and the wavelength of the fluctuation is about 2.5 km. This corresponds to the fastest growing mode (the wavelength approximately 7.5 times the sheet-width; Miles and Howard 1964) of the horizontal shear layer for linear theory. Vortices embedded in the vortex sheet are not associated with cumuli or cumulonimbi, except for the most developed vortex which is colocated with the supercell storm. This result suggests that the horizontal shear instability may largely contribute the generation and development of the low-level vortices.

6. Generation and development processes of tornadoes

In order to understand the vorticity dynamics associated with tornadogenesis, we break the three-dimensional vorticity equation into vertical and horizontal components, as in Klemp and Rotunno (1983). The vertical vorticity equation is given by

$$\frac{d\zeta}{dt} = \omega_h \cdot \nabla w + \zeta \frac{\partial w}{\partial z} + F_\zeta, \qquad (1)$$

where the first and second terms on the right-hand side are the tilting and stretching terms, respectively. The horizontal vorticity equation is given as

$$\frac{d\omega_h}{dt} = \omega \cdot \nabla \mathbf{V}_h + \nabla \times (B\mathbf{k}) + F_{\omega_h}, \qquad (2)$$

where the first and second terms on the right-hand side are the tilting and solenoidal terms, respectively.

In order to examine the generation and development processes of simulated tornado vortices, a trajectory analysis around the tornado is performed, as in Wicker and Wilhelmson (1995). At 0745 JST, a horizontal ring of 50 parcels is placed around the center of the tornado at a radius of 150 m and a height of 150 m. These particles are then integrated backward in time to 0735 JST to determine the source regions for air.

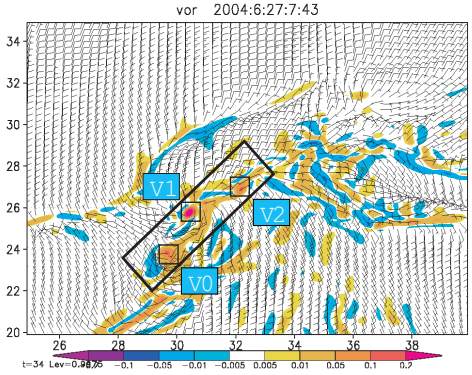

(a) 0743 JST

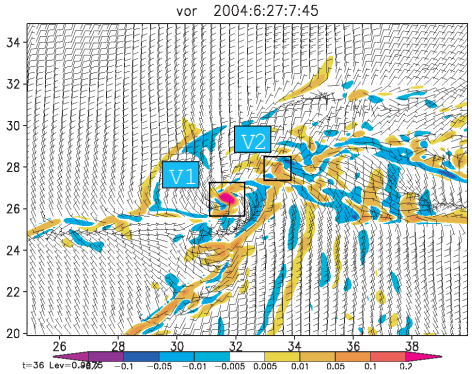

(b) 0745 JST

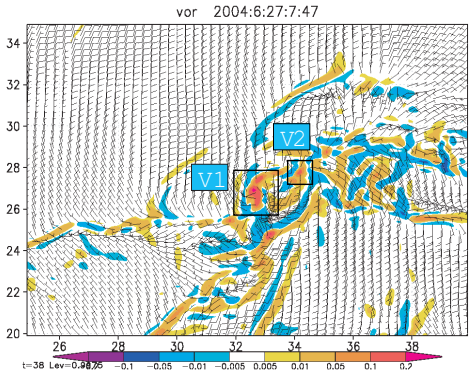

(c) 0747 JST

Figure 5: Horizontal cross section of the vertical vorticity and horizontal wind fields near the surface from DOMAIN 5 at (a) 0743 JST, (b) 0745 JST, (c) 0747 JST. The vertical vorticity field is indicated by shaded area and the horizontal wind field is indicated by barbs. A 15 km ×15 km portion of the full domain is shown.

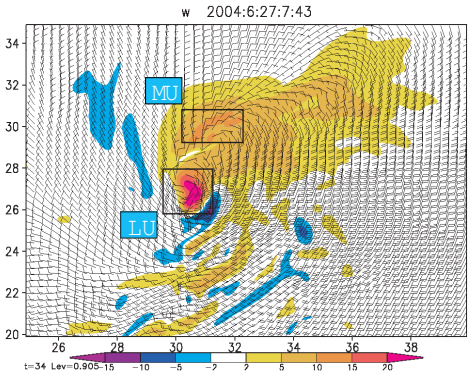

(a) 0743 JST

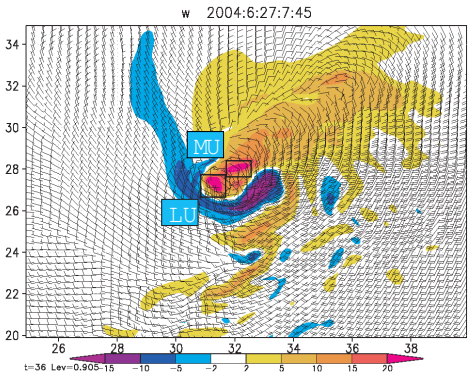

(b) 0745 JST

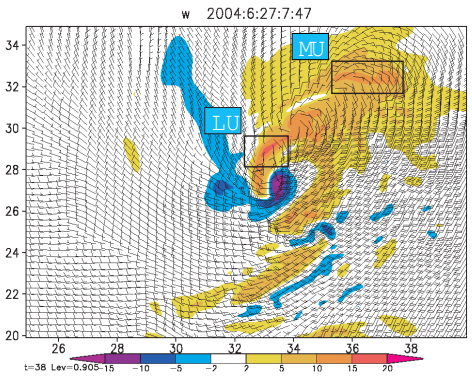

(c) 0747 JST

Figure 6: Same as Fig. 5 except for the vertical velocity (shaded) and the horizontal wind (barbs) fields at z = 1 km.

Figure 7 shows a set of backward-trajectories. The trajectories indicate that the tornado air originates primarily from two source regions. One region is north-northeast of the tornado. Figure 8a shows the stretching and tilting terms along the representative parcel's path from this region. This parcel originates about 8.5 km north-northeast of the tornado near a height of 200 m and travels south-southwestward, and once descends to near the surface and subsequently rises as they approach into the tornado cyclonically. As the parcel moves near the tornado, it enters the region of maximum θ_e gradient (not shown). After 0744 JST, the parcel undergoes the solenoidal generation of horizontal vorticity, and subsequently undergoes the generation of vertical vorticity by tilting of horizontal vorticity. This vertical vorticity is stretched and intensified by the storm updraft.

The other source region for parcels is located northeast of the tornado. Figure 8b shows the stretching and tilting terms along the representative parcel's path from this region. This parcel originates about 5.5 km northeast of the tornado near the surface and travels southwestward and rises as they approaches into the tornado cyclonically. As the parcel moves near the tornado, it enters the horizontal shear zone (not shown). After 0743 JST, a parcel undergoes the generation of vertical vorticity without tilting and solenoidal effects. This parcel travels along the horizontal shear zone so that the generation of vertical vorticity may be due to the horizontal shear instability. This vertical vorticity is stretched and intensified by the storm updraft.

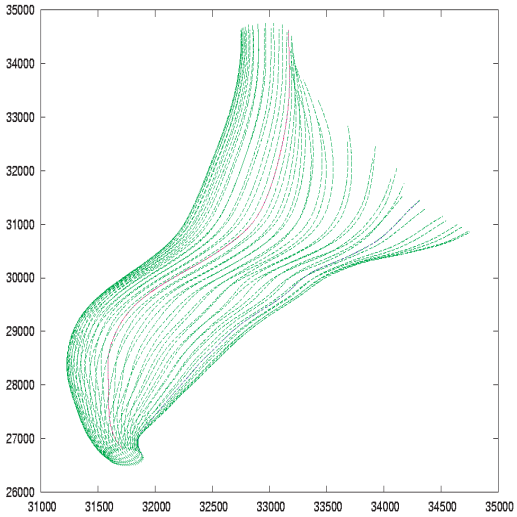

Figure 7: Backward trajectories from 0745 JST to 0735 JST for 50 parcels. These parcels are placed around the center of the tornado at a radius of 150 m and a height of 150 m.

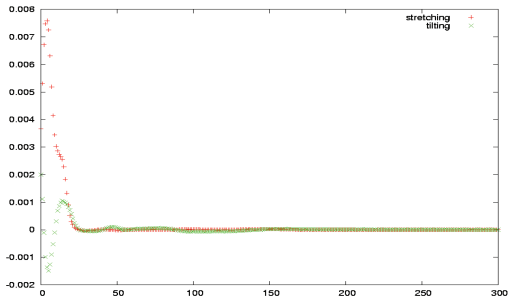

(a) First source region

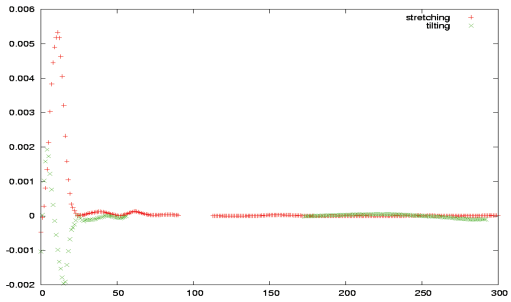

(b) Second source region

Figure 8: Time series of the stretching and tilting terms along the representative trajectories of each source region in Fig. 7.

7. Summary and discussion

We succeed in simulating tornadoes associated with a supercell using a super-high resolution (horizontal resolution $\sim$ 100 m) model with realistic conditions.

The simulated tornadic supercell results from the merger of two cells. After the merger, the low-level vortex rapidly intensifies and reaches 0.58 s^{-1}. At the same time, the horizontal wind speed exceeds 37 m s^{-1}, which is beyond the criteria of F1 tornado. The cell merger may play a role in the development of the tornadic vortex.

It is found that a preexisting boundary accompanied by the horizontal wind shear and convergence interacts with the mid-level mesocyclone. The preexisting boundary fluctuates with wavelength of 2.5 km, which corresponds to that of the fastest growing mode of the horizontal shear instability for linear theory. When one of the low-level vortices on the preexisting boundary is coupled with the mid-level mesocyclone, it intensifies into the tornadic vortex.

A trajectory analysis shows that the tornadic vor-

tex undergoes two types of generation and development processes. One contains tilting of the baroclinically generated horizontal vorticity and subsequent stretching by the storm updraft. This corresponds to the process of tornadogenesis associated with supercells reported by Klemp and Rotunno (1983) and Wicker and Wilhelmson (1995). The other process is as follows; the low-level vortices are generated on the preexisting boundary due to the horizontal shear instability, and subsequently one of the vortices is stretched by the strong updraft associated with the mid-level mesocyclone. This is similar to the process of tornadogenesis presented by Wakimoto and Wilson (1989) and Lee and Wilhelmson (1997a,b), except for the presence of the mid-level mesocyclone. Thus, the tornadogenesis of the simulated tornadic vortex is a "hybrid" category with the interaction between the mid-level mesocyclone and the low-level vortex intensified due to the horizontal shear instability.

Acknowledgments. The authors wish to thank to the office of Saga Prefecture, the agricultural research center of Saga, the office of Saga-Higashi high school and Saga Local Meteorological Observatory for providing observation data. We are also deeply grateful for beneficial suggestions and discussion.

References

Alexander, C. R., and J. Wurman, 2004: The 30 May 1998 Spencer, South Dakota, Storm. Part I: The structural evolution and environment of the tornadoes. *Mon. Wea. Rev.*, **133**, 72-96.

Atkins, N. T., M. L. Weisman, and L. J. Wicker, 1999: The influence of preexisting boundaries on supercell evolution. *Mon. Wea. Rev.*, **127**, 2910-2927.

Burgess, D. W., 1997: Tornado warning guidance. *OSB/OTB*, Oklahoma, 28pp.

Doswell, C. A. III, and D. W. Burgess, 1993: Tornadoes and tornadic storms: A review of conceptual models. *The Tornado: Its Structure, Dynamics, Prediction, and Hazards, Geophys. Monogr.*, No. 79, Amer. Geophys. Union, 161-172.

Dowell, D. C., and H. B. Bluestein, 2002: The 8 June 1995 McLean, Texas, Storm. Part I: Observations of cyclic tornadogenesis. *Mon. Wea. Rev.*, **130**, 2626-2648.

———, and ———, 2002: The 8 June 1995 McLean, Texas, Storm. Part II: Cyclic tornado formation, maintenance, and dissipation. *Mon. Wea. Rev.*, **130**, 2649-2670.

Hong, S.-Y., and H.-L. Pan, 1996: Nonlocal boundary layer vertical diffusion in a medium-range forecast model. *Mon. Wea. Rev.*, **124**, 2322-2339.

Klemp, J. B., and R. Rotunno, 1983: A study of the tornadic region within a supercell. *J. Atoms. Sci.*, **40**, 359-377.

Lee, B. D., and R. B. Wilhelmson, 1997: The numerical simulation of non-supercell tornadogenesis. Part I: Initiation and evolution of pretornadic misocyclone circulations along a dry outflow boundary. *J. Atmos. Sci.*, **54**, 32-60.

———, and ———, 1997: The numerical simulation of non-supercell tornadogenesis. Part II: Evolution of a family of tornadoes along a weak outflow boundary. *J. Atmos. Sci.*, **54**, 2387-2415.

Moller, A. R., C. A. Doswell III, M. P. Foster, and G. R. Woodall, 1994: The operational recognition of supercell Thunderstorm environments and storm structures. *Wea. Forecasting*, **9**, 327-374.

Tao, W. K., and J. Simpson, 1993: Goddard Cumulus Ensemble Model. Part I: Model Description. *Terrestrial, Atmospheric and Oceanic Sciences*, **4**, 35-72.

Wakimoto, R. M., and C. Liu, 1998: The Garden City, Kansas, storm during VORTEX 95. Part II: The wall cloud and tornado. *Mon. Wea. Rev.*, **126**, 393-408.

———, C. Liu, and H. Cai, 1998: The Garden City, Kansas, storm during VORTEX 95. Part I: Overview of the storm's life cycle and mesocyclogenesis. *Mon. Wea. Rev.*, **126**, 372-392.

———, and J. W. Wilson, 1989: Non-supercell tornadoes. *Mon. Wea. Rev.*, **117**, 1113-1140.

Wicker, L. J., and R. B. Wilhelmson, 1995: Simulation and analysis of tornado development and decay within a three-dimensional supercell thunderstorm. *J. Atoms. Sci.*, **52**, 2675-2703.